



Thermal and spectroscopic studies of 2,3,5-trisubstituted and 1,2,3,5-tetrasubstituted indoles as non-competitive antagonists of GluK1/GluK2 receptors

Agata Bartyzel¹ · Agnieszka A. Kaczor^{2,3} · Halina Głuchowska¹ · Monika Pitucha⁴ · Tomasz M. Wróbel^{2,5} · Dariusz Matosiuk²

Received: 16 November 2017 / Accepted: 27 February 2018 / Published online: 8 March 2018

© The Author(s) 2018. This article is an open access publication

Abstract

This paper reports the thermal stability and thermal degradation of six derivatives of indole by means of TG-DSC (in air) and TG-FTIR (in nitrogen) techniques. The compounds were also characterized by infrared spectroscopy. In addition, IR spectra were calculated and compared with the experimental data. In particular, the potential energy distribution analysis was performed to assign IR signals. The studied compounds are characterized by good thermal stability in oxidizing and inert atmospheres which is important for potential medical application. Thermogravimetric measurements in air atmosphere showed that the decomposition of compounds proceeds in two or three main stages. The thermal degradation of compounds is preceded by the melting process. The pyrolysis of samples is a one-step process. Together with the analyses performed in nitrogen, the FTIR spectra of the evolved gas phase products were recorded. On the FTIR spectra of gaseous products, only the bands of water, carbon dioxide and carbon oxide molecules are present. In the case of indole derivatives containing the *p*-chlorobenzyl substituent in position 1, the bands of anisole, *p*-chlorotoluene and chlorobenzene also appear.

Keywords Indole derivatives · Thermal behaviour · IR spectra · PED analysis · Theoretical computations · Non-competitive antagonists of GluK1/GluK2 receptors

Introduction

Indole is a well-known and important privileged structure scaffold found in many natural and synthetic compounds. This core is recognized as one of the foremost biologically significant moieties in nature. The indoles are characterized

by excellent binding affinity for various receptors [1, 2]. The indole-based compounds can also exhibit various biological activities such as anti-inflammatory, analgesic, antifungal, antimicrobial, insecticidal, antioxidant, antiviral, antidepressant, antiarrhythmic, antihistaminic and antidiabetic ones. [3–6]. According to the literature, there are over ten thousand biologically active compounds containing indole core. More than 200 of them were approved as commercially available drugs or are undergoing clinical

Electronic supplementary material The online version of this article (<https://doi.org/10.1007/s10973-018-7146-6>) contains supplementary material, which is available to authorized users.

✉ Agata Bartyzel
agata.bartyzel@poczta.umcs.lublin.pl

¹ Department of General and Coordination Chemistry, Maria Curie-Skłodowska University, Maria Curie-Skłodowska Sq. 2, 20031 Lublin, Poland

² Department of Synthesis and Chemical Technology of Pharmaceutical Substances with Computer Modeling Laboratory, Faculty of Pharmacy with Division of Medical Analytics, Medical University, 4a Chodzki St., 20093 Lublin, Poland

³ Department of Pharmaceutical Chemistry, School of Pharmacy, University of Eastern Finland, Yliopistonranta 1, P.O. Box 1627, FI-70211 Kuopio, Finland

⁴ Department of Organic Chemistry, Faculty of Pharmacy with Division of Medical Analytics, Medical University, 4a Chodzki St., 20093 Lublin, Poland

⁵ Department of Drug Design and Pharmacology, Faculty of Health and Medical Sciences, University of Copenhagen, Universitetsparken 2, 2100 Copenhagen Ø, Denmark

trials [7, 8], e.g., vinblastine (anticancer), indomethacin (anti-inflammatory), arbidol (antiviral), delavirdine (anti-HIV), zafirlukast (anti-asthmatic), pravadoline (analgesic), bucindolol (β -blocker) and roxindole (schizophrenia) [4–6]. The indoles are also used as dyes, pigments, plastics, fungicides, vitamin supplements, flavour enhancers, and perfumery [9].

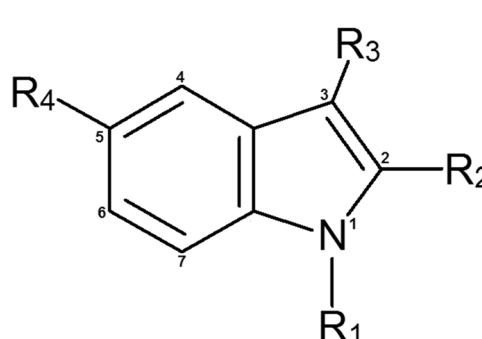
The main aim of this research was the thermal and spectroscopic characterization of six indole derivatives, i.e., 5-methoxy-2-(4-methoxyphenyl)-3-methylindole (**1**), 1-ethyl-5-methoxy-2-(4-methoxyphenyl)-3-methylindole (**2**), 1-[(4-chlorophenyl)methyl]-5-methoxy-2-(4-methoxyphenyl)-3-methylindole (**3**), 1-ethyl-2-(4-methoxyphenyl)-3-methylindole (**4**), 1-ethyl-2-phenyl-5-methoxy-3-methylindole (**5**) and 11-ethyl-8-methoxy-6,11-dihydro-5*H*-benzo[*a*]carbazole (**6**) (Scheme 1). The investigated compounds were synthesized in the Fisher indolization reaction from the respective arylhydrazine hydrochloride and appropriate ketone in anhydrous boiling ethanol saturated with HCl followed by alkylation with alkyl halide (with application of sodium hydride). These compounds are a non-competitive antagonists of kainate GluK1/GluK2 (GluK—glutamatergic kainate receptors) receptors with low micromolar activity, and compound **2** is the most promising from the series [10, 11]. Non-competitive antagonists of kainate receptors [10–15] can be considered promising compounds for the treatment of neurodegenerative diseases [16, 17] as well as epilepsy [18]. In particular, a non-competitive mode of action can result in a better safety profile as reported for non-competitive antagonists of α -amino-3-hydroxy-5-methyl-4-isoxazolepropionic acid (AMPA) receptors [19]. In the previous studies, we also constructed 3D models of GluK1 and GluK2 receptors and suggested that indole-derived non-competitive antagonists can bind in the receptor transduction domain [11, 14, 15, 20, 21]. In this study, in

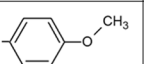
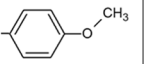
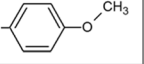
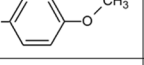
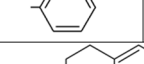
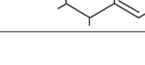

order to investigate thermal behaviour of indole derivatives the TG-DSC and TG-FTIR methods were applied. The compounds were also characterized by infrared spectroscopy. In addition, infrared (IR) spectra of the studied indole derivatives were calculated and compared with the experimental data. Theoretical vibrational spectra of the compounds were interpreted in terms of potential energy distribution (PED) analysis. Shortly, in order to describe the vibration of a *N*-atomic molecule using the PED analysis, the construction of the set of $3N-6$ local, linearly independent, internal coordinates is required [22]. This set represents stretching, bending and deformation motions of the functional groups or the chosen fragments of the molecule [22]. The availability of such a coordination set instead of the normal modes causes that the potential energy distribution matrix, the PED matrix, ceases to be diagonal, but the energy distribution originating from the motions of particular functional groups is understandable for the interpreter [22]. The rationale of the performed research results from the necessity of thermal stability of the compounds under investigations which is important for their potential biomedical application.

Experimental

Synthesis and short description of compounds 1–6

The investigated compounds were synthesized according to the following procedure: the mixture of 0.05 mol of arylhydrazine hydrochloride, 0.05 mol of ketone, 100 cm³ of anhydrous ethanol and 10 cm³ of ethanol saturated with HCl was refluxed for 4 h. The reaction mixture was left overnight at room temperature. The obtained product was



Compound	R ₁	R ₂	R ₃	R ₄
1	-H		-CH ₃	-OCH ₃
2	-C ₂ H ₅		-CH ₃	-OCH ₃
3			-CH ₃	-OCH ₃
4	-C ₂ H ₅		-CH ₃	-H
5	-C ₂ H ₅		-CH ₃	-OCH ₃
6	-C ₂ H ₅			-OCH ₃

Scheme 1 The studied indoles

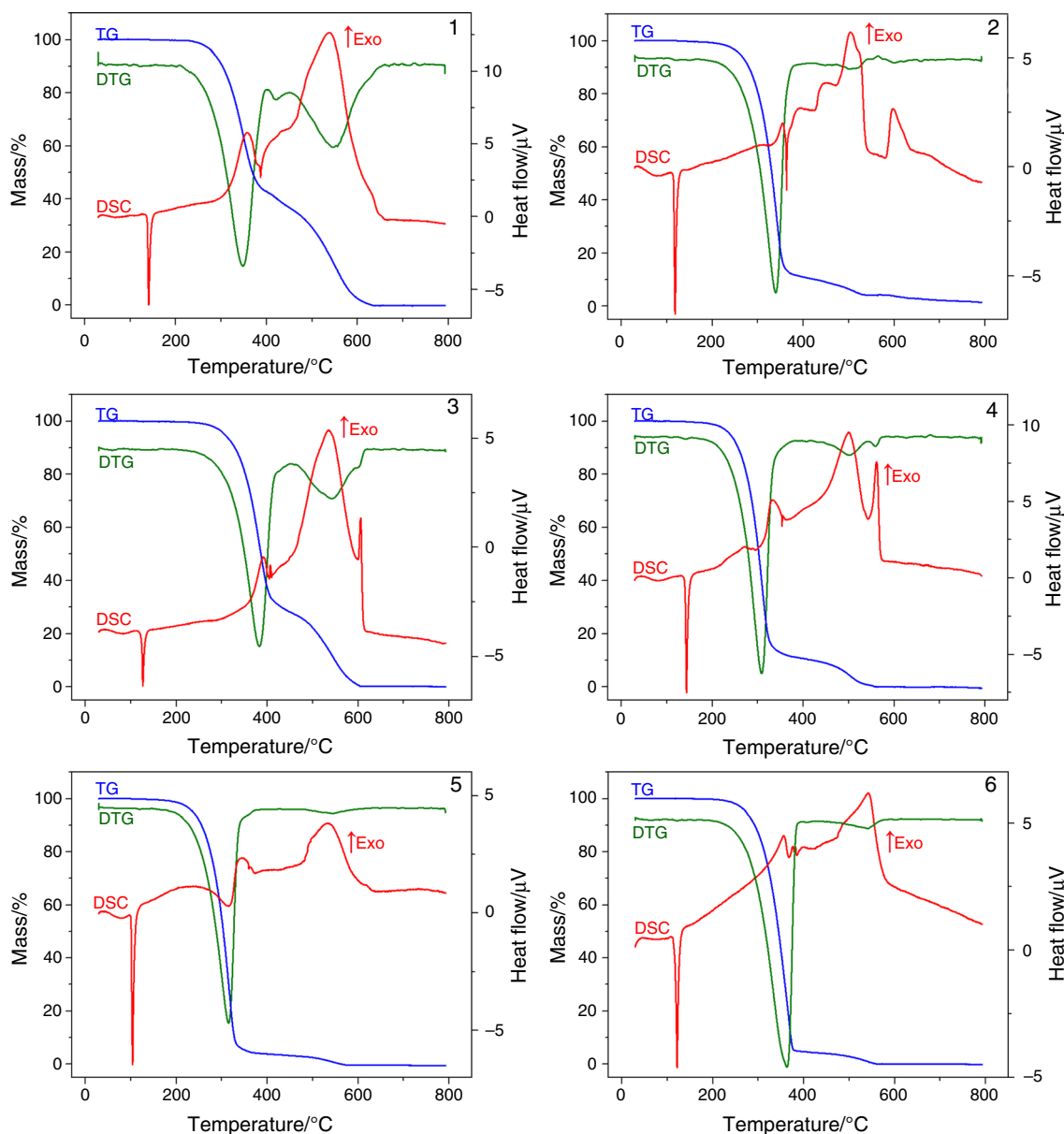


Fig. 1 TG, DTG and DSC curves recorded for 1–6 in air atmosphere

Table 1 Results of the melting process

Sample	$T_{\text{onset}}/^{\circ}\text{C}$	$T_{\text{peak}}/^{\circ}\text{C}$	$\Delta H_{\text{m}}/\text{J g}^{-1}$	$\Delta H_{\text{m}}/\text{J mol}^{-1}$
1	137	141	82.21	21.98
2	115	118	71.92	21.23
3	124	127	48.94	19.14
4	140	143	82.64	21.91
5	100	104	71.02	18.83
6	117	122	69.51	19.26

filtered and purified by crystallization from ethanol and washed with *n*-hexane. In the next step, 0.01 mol of the indole derivative was dissolved in 30 cm³ of anhydrous

N,N-dimethylformamide (DMF). The reaction mixture was cooled to 0 °C, and 0.8 g of sodium hydride was added (50% oil suspension). After 30 min of mixing, a solution of 0.012 mol of alkyl halide in 20 cm³ of anhydrous DMF was added dropwise. The reaction was allowed to continue at room temperature for 3 h. The mixture was filtered, and 30–40 cm³ of water was added to the filtrate. The obtained precipitate was filtered off and purified by crystallization from ethanol and washed with *n*-hexane. The detailed physicochemical and spectral properties of the investigated compounds were described in the previous paper [10].

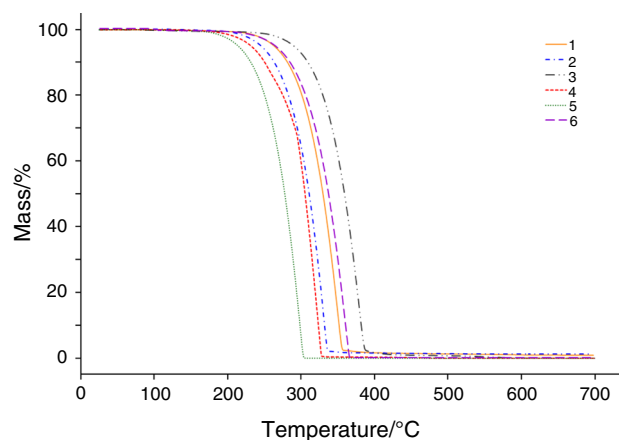
Table 2 Thermal analysis data for compounds **1–6**

Complex	Atm	Temperature range/°C	$T_{peak}/^{\circ}\text{C}$	Mass loss/%
1	Air	222–398	348	56.98
		398–652	421; 548	43.02
2	Air	205–398	339	89.97
		398–537	503; 515	5.81
		587–787	600	2.73
3	Air	193–360	331; 346	98.46
		251–435	383	70.40
4	Air	435–612	542; 598	29.58
		234–444	379	99.00
		182–381	309	88.73
5	Air	381–540	503	10.40
		540–570	559	0.84
		167–334	256; 344	99.52
6	Air	182–384	315	95.93
		484–603	544	4.07
6	Air	164–310	299	99.94
		217–390	363	95.09
		463–575	543	4.90
6	N ₂	200–370	360	99.93

Atm atmosphere of analysis, T_{peak} DTG peak temperature (maximum change of mass)

Methods and physical measurements

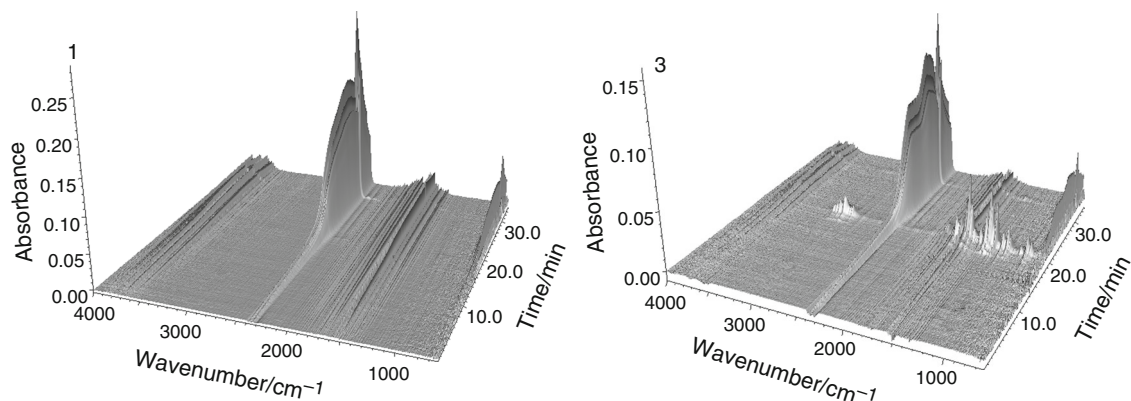
The thermal behaviour of compounds was studied in air and nitrogen atmospheres. The thermal stability and decomposition in oxidizing atmosphere were determined using the Setaram Setsys 16/18 derivatograph. The TG and DSC curves were recorded in temperature range between 30 and 800 °C. The samples (6.18–7.56 mg) were heated in a ceramic crucible at the heating rate of 10 °C min⁻¹ in flowing air ($v = 0.75 \text{ dm}^3 \text{ h}^{-1}$). The temperature and heat flow of the instrument were calibrated by the melting point

**Fig. 2** TG curves of **1–6** in nitrogen

and enthalpy of indium standard. The studies in inert atmosphere were carried out using the TGA Q5000 analyser (TA Instruments, New Castle, Delaware, USA). The compounds (15.14–29.69 mg) were heated in an open platinum crucible from ambient temperature ($\sim 23\text{--}25 \text{ }^{\circ}\text{C}$) to 700 °C in flowing nitrogen ($25 \text{ cm}^3 \text{ min}^{-1}$). Simultaneously with the TG analysis in nitrogen, the infrared spectra of gaseous products were recorded using the Nicolet 6700 FTIR spectrophotometer (Thermo Scientific) in the spectral range of 600–4000 cm^{-1} with a resolution of 4 cm^{-1} and 6 scans per spectrum. ATR-FTIR spectra were collected using the Thermo Scientific Nicolet 6700 FTIR spectrometer equipped with a Smart iTR diamond ATR accessory in the range from 4000 to 500 cm^{-1} . The samples were placed directly on the diamond crystal of ATR accessory, and the spectra were obtained from 16 scans taken at a resolution of 4 cm^{-1} and normalized.

Computational studies

Energy and geometry of compounds **1–6** were optimized with the B3LYP DFT method (DFT—density functional

**Fig. 3** 3D FTIR spectra of pyrolysis products during the thermal degradation of **1** and **3**

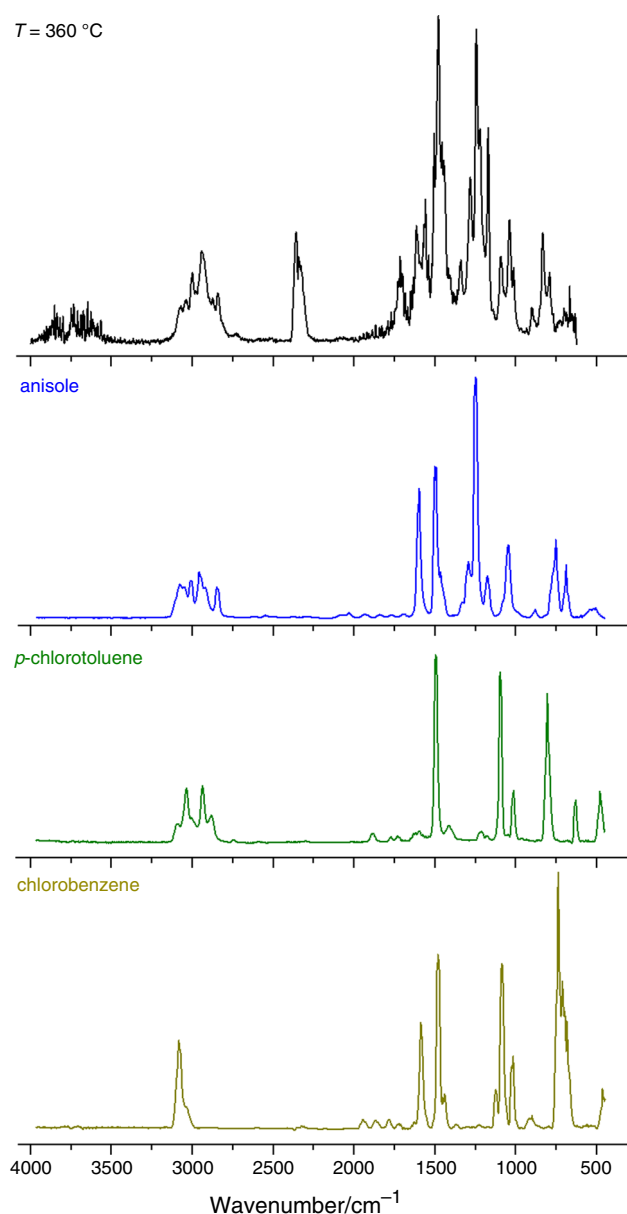


Fig. 4 FTIR spectrum of volatile products of thermal decomposition of **3** recorded at 360 °C and the spectra of anisole, *p*-chlorotoluene and chlorobenzene

theory) and the 6-311G++(2df, 2pd) basis set of Gaussian09 software [23]. Gaussian09 was also used to calculate IR spectra. The computed IR spectra were corrected using the scaling factor of 0.962 as recommended for this level of theory [24]. Moreover, the computed vibrational frequencies have been unambiguously assigned by means of the potential energy distribution (PED) analysis of all the fundamental vibration modes by using VEDA 4 program [25, 26] as described previously [27–30].

Results and discussion

Thermal behaviour of 1–6

The TG-DSC curves providing information about the thermal properties of **1–6** are shown in Fig. 1. As it can be seen in the TG curves, the compounds are characterized by good thermal stability, which is a very important parameter for their potential application as drugs. The first changes are recorded on the DSC curves as endothermic peaks at temperature 100–140 °C. These peaks are not accompanied by a mass loss and can be attributed to the melting process. They are roughly similar to the values reported earlier and determined using a Boetius apparatus [10]. The melting point onset temperature (T_{onset}), peak temperature (T_{peak}) corresponding to each peak, and enthalpy of fusion taken from the DSC curves for all compounds are listed in Table 1. The melting peaks are sharp which indicates that the compounds were probably synthesised as pure, crystalline substances [31–33]. Generally, the substitution of the pyrrole hydrogen atom in position 1 leads to a decreased melting point. The exception is compound **4** where the melting point is comparable to that of compound **1**. This can be a result of a lack of a substituent in the 5-position of the indole core.

The decompositions of the compounds in air are two- or three-step processes that are noted on the TG curves (see Fig. 1). For all compounds, the major mass loss (56.98–95.93%) occurs in the first stage which starts at 183–251 °C (Table 2). Taking into account the initial temperature of the decomposition processes, the following relative thermal stability order: $5 = 4 < 2 < 6 < 1 < 3$ can be established. As can be observed, the substitution of hydrogen attached to nitrogen atom with the ethyl group decreases the combustion temperature of compounds while the *p*-chlorobenzyl substituent stabilizes the molecule and increases the decomposition temperature of **3** in air compared to **1**. In the case of compounds **1** and **3**, probably during the first stage the substituents of the indole core are broken off and combusted. The theoretical values of the indole residue ($\text{C}_8\text{H}_7\text{N}$) are 43.82 and 29.95% while the experimental ones are equal to 43.03 and 29.60% for compounds **1** and **3**, respectively. The formed products are unstable and immediately undergo complete destruction and combustion accompanied by a significant exothermic effect. The samples are fully decomposed at 612–652 °C. It is worth mentioning that for compound **1** on the DTG curve two maxima are visible during this stage, but this is not clearly indicated on the TG curve. The remaining compounds are almost completely decomposed during this step (more than 85% of overall mass is lost), and the formed residues are combusted during one (**5** and **6**) or two (**2** and

Table 3 Experimental and computed IR frequencies and PED assignment of signals for compound **2** (the most promising compound within the studied series)

Experimental	Computed		
	Raw	Scaled	PED
	3241	3117	ν CH (99)
	3215	3092	ν CH (94)
	3211	3089	ν CH (92)
	3197	3075	ν CH (99)
	3189	3068	ν CH (99)
	3182	3061	ν CH (92)
	3180	3059	ν CH (94)
	3177	3056	ν CH (99)
	3135	3015	ν CH (92)
	3124	3005	ν CH (99)
2996 (m)	3123	3004	ν CH (92)
	3103	2985	ν CH (99)
	3100	2982	ν CH (83)
2951 (m)	3066	2949	ν CH (100)
	3055	2939	ν CH (88)
2830 (w)	3051	2935	ν CH (99)
1898 (vw)	3037	2922	ν CH (99)
1868 (vw)	3009	2895	ν CH (92)
1835 (vw)	2999	2885	ν CH (93)
1612 (m)	1658	1595	ν CC (60)
1588 (w)	1650	1587	ν CC (31)
1576 (w)	1610	1549	ν CC (19)
1562 (w)	1604	1543	ν CC (35)
1506 (m)	1580	1520	ν CC (45)
1481 (s)	1538	1480	δ HCC (12)
	1513	1456	δ HCH (53)
	1510	1454	δ HCH (45)
1448 (s)	1507	1448	δ HCH (61), Γ HCOC (10)
	1502	1445	δ HCH (12)
	1497	1440	δ HCH (70)
	1496	1439	δ HCH (75), Γ HCOC (16)
	1495	1438	δ HCH (78), Γ HCOC (14)
1431 (m)	1493	1436	δ HCH (72), Γ HCCN (15)
	1481	1425	ν CC (33), δ HCC (10)
	1479	1423	δ HCC (76)
1418 (m)	1473	1417	δ HCC (10), δ HCH (48)
1386 (m)	1446	1391	ν CC (32), δ HCC (22)
1377 (w)	1421	1367	δ HCC (17)
1366 (m)	1412	1358	δ HCH (82)
1351 (m)	1400	1347	δ HCH (15), Γ HCNC (30)
	1374	1322	ν NC (26)
1307 (m)	1356	1304	ν CC (33), δ HCC (12)
1286 (s)	1337	1286	δ HCC (72)
	1325	1275	δ CCC (10)
	1318	1268	ν CC (17), δ CCC (11)
1246 (s)	1303	1253	δ HCC (22), Γ HCNC (10)
1231 (vs)	1276	1228	ν CC (28), ν OC (32)
	1261	1213	ν CC (11), δ HCC (10)

Table 3 continued

Experimental	Computed		
	Raw	Scaled	PED
1202 (s)	1251	1203	ν OC (20), δ HCC (28)
1182 (m)	1213	1167	ν OC (26)
1171 (s)	1205	1159	δ HCH (17), Γ HCOC (58)
	1201	1155	δ HCH (10), Γ HCOC (32)
1142 (m)	1198	1153	δ HCC (51)
	1174	1130	ν CC (15), δ HCC (36)
	1173	1128	δ HCH (29), Γ HCOC (67)
1108 (m)	1166	1122	δ HCC (26)
	1134	1091	δ HCC (25)
1072 (s)	1096	1054	ν CC (19), Γ HCCN (39)
1035 (vs)	1067	1027	ν OC (64)
	1064	1024	ν OC (53), δ HCC (13)
1003 (w)	1025	986	δ CCC (43)
963 (vw)	993	955	Γ HCCC (70), Γ CCCC (13)
948 (w)	969	932	Γ HCCC (71)
	955	919	ν CC (44), δ CCC (15)
	950	914	ν CC (45), δ CCN (12)
895 (m)	927	892	Γ HCCC (85), Γ CCCC (11)
848 (m)	887	853	Γ HCCC (71)
833 (s)	868	835	Γ HCCC (65)
818 (s)	862	829	Γ HCCC (54), Γ OCCC (17)
794 (vs)	832	800	Γ HCCC (100)
	810	779	Γ HCCC (48)
775 (m)	807	776	ν CC (24), ν OC (14), Γ HCCC (11)
	797	766	Γ HCCC (84)
	785	755	ν NC (11), Γ HCCN (10)
	780	750	ν CC (13), δ CCC (12)
738 (w)	761	732	Γ CCCC (69)
702 (m)	752	723	Γ CCCC (34)
	699	672	Γ CNCC (34)
658 (w)	675	649	ν NC (11), Γ CNCC (12)
630 (m)	654	629	δ CCC (11)
617 (w)	642	617	δ CCC (31), Γ CNCC (10)
606 (m)	632	608	Γ HCCC (14), Γ CCCC (34), Γ OCCC (20)
583 (w)	597	574	δ CCC (12), δ OCC (11)
564 (w)	575	553	Γ OCCC (10)
526 (vw)	551	530	δ CCC (14), δ COC (21)
	519	499	Γ OCCC (20)
	488	469	δ OCC (21), δ COC (18)
	470	452	δ CCN (21)
	447	430	Γ HCCC (11), Γ CCNC (14), Γ CCCC (36), Γ OCCC (13)
	433	417	Γ HCCC (32), Γ CCCC (58)
	404	389	δ COC (10)
	366	352	δ CCN (23), Γ CNCC (10)
	359	345	δ COC (10), Γ OCCC (11), Γ CCCC (10)
	337	324	δ CCC (12), Γ CCCN (15), Γ OCCC (16)
	311	299	δ CNC (26), Γ HCCN (10)
	265	255	δ OCC (20), δ COC (13), Γ CCNC (10)

Table 3 continued

Experimental	Computed		
	Raw	Scaled	PED
	250	241	Γ HCOC (64)
	228	219	δ OCC (14), Γ HCOC (10), Γ HCCN (13)
	213	205	ν CC (19), δ CCC (11)
	195	188	δ CNC (19), Γ HCCN (11)
	190	183	δ OCC (13), Γ CCNC (14)
	147	141	δ CCC (10), Γ COCC (10)
	95	91	Γ COCC (55)
	81	78	Γ COCC (25), Γ CCCN (35)
	67	64	Γ COCC (27), Γ CCNC (11), Γ CCCN (22)
	60	58	Γ NCCC (44), Γ CCCC (10)
	55	53	Γ COCC (13), Γ CCNC (39)
	37	36	δ NCC (14), δ CCC (16), Γ CNCC (18), Γ NCCC (22)
	32	31	Γ CNCC (18), Γ NCCC (13), Γ CCCC (23)

s Strong, *m* medium, *w* weak, *v* very, *br* broad, *sh* shoulder, ν stretching, δ bending in plane, Γ torsional vibrations

4) steps. Compounds **4**, **5** and **6** are fully combusted at a temperature of 570–603 °C. In the case of **2**, it was found that under the measuring conditions a small amount of unburnt organic matrix remains (1.49%).

Thermal behaviour of **1–6** was also studied in nitrogen atmosphere (see Fig. 2). The order of thermal stabilities in inert and oxidizing atmospheres is similar; taking into account the initial temperature of the decomposition processes under nitrogen stream, the following relative thermal stability order: $5 \approx 4 < 2 < 6 < 1 < 3$ can be established. In contrast to the thermal decomposition in air, the pyrolysis processes start at a lower temperature (about 12–22 °C) than the combustion ones. Thermal decompositions of compounds in nitrogen proceed in one major mass loss step and similar to the combustion, the compounds are almost completely burnt (for compound **2** the residue after the pyrolysis is 1.54%). The total pyrolysis of the compounds can be associated with the presence of methoxy groups as observed for other compounds containing such substituent [30, 31]. Simultaneously with the TG analysis in nitrogen, the FTIR spectra of gaseous products were recorded. The FTIR spectra of gaseous products evolved during the decomposition of compounds **1** and **3** are given in Fig. 3. In the spectra of gaseous products, except for the compound **3**, only the bands characteristic of water, carbon monoxide and carbon dioxide were present. The peaks at 2240–2400 cm^{-1} are assigned to stretching vibration $\nu(\text{C}=\text{O})$ of carbon dioxide molecule. In addition, a band at 669 cm^{-1} is observed due to the deformation vibration of CO_2 . The double peaks in the range 2050–2275 cm^{-1} correspond to the vibrations of CO molecule. The characteristic bands of water molecules are observed in the range 3450–4000 and 1300–1950 cm^{-1}

for stretching and deformation vibrations, respectively [31, 32, 34]. Probably other compounds such as indole can be condensed in the transfer line and do not reach the detector. In the case of compound **3**, at a temperature between 340 and 420 °C of the pyrolysis process on the FTIR spectra of evolved gases, several bands in the range 2700–3100 and 750–1800 cm^{-1} were recorded. These peaks are probably due to the presence of anisole, *p*-chlorotoluene and chlorobenzene (see Fig. 4).

Infrared spectroscopy

The FTIR spectra of **1–6** are given in Figs. S1–S6. The observed and calculated frequencies in the infrared spectra of studied compounds together with their PED assignment of signals are presented in Tables 3 and S1–S5 (Supplementary material). The scaled computed IR spectra are in accordance with the experimental values. The strong, sharp peak at 3379 cm^{-1} in the FTIR spectrum of **1** is characteristic of $\nu(\text{N}-\text{H})$ vibrations of the pyrrole ring. This is consistent with the literature data; the indoles unsubstituted in the 1-position (N) give a sharp absorption peak in the range 3500–3300 cm^{-1} [35–40]. This band was not recorded in the spectra of other studied compounds due to the substitution of hydrogen atom in position 1 by ethyl or 4-chlorobenzyl group. The peaks at 3100–2990 cm^{-1} can be assigned to the C–H stretching vibrations of the aromatic bonds. The symmetric and asymmetric C–H stretching bands of the methyl/ethyl groups are observed in 2990–2800 cm^{-1} . The other important peaks are observed at the range 1620–1400 cm^{-1} , and they are mainly due to the stretching vibrations $\nu(\text{CC})$ of indole and benzene rings. The varying intensity bands observed in the FTIR spectra

at 1373–1342 and 1287–1283 cm^{-1} can be assigned to the C–N stretching modes of pyrrolic ring. These assignments are in agreement with the literature [35, 39, 41] and correlate with the theoretical calculations. The remaining bands characteristic of **1–6** with their detailed description is given in Tables 3 and S1–S5.

Conclusions

Thermal analysis of six indoles derivatives was performed. The investigated compounds are stable at room temperature which is important for their medical application. The DSC melting peaks of compounds are sharp indicating that they are probably crystalline, pure substances. In air atmosphere, the decomposition process of **1–6** occurs in two or three stages where the main mass loss occurs during the first one. On the basis of the TG-DSC analysis, it can be concluded that the substitution of hydrogen atom by the ethyl group on the pyrrole ring in 1 position leads to decrease in the thermal stability of the studied indoles. Changing the substituent to the *p*-chlorobenzyl group causes the compound stabilization and, consequently, an increase in the decomposition temperature of **3** compared to that of the other compounds. The performed TG-FTIR analysis showed there are no residual solvents in the structure of studied compounds.

Acknowledgements The paper was developed using the equipment purchased within the projects “The equipment of innovative laboratories doing research on new medicines used in the therapy of civilization and neoplastic diseases” and “Enhancement of the Research and Development Potential of the UMCS Faculty of Chemistry and the Faculty of Biology and Earth Sciences” within the Operational Program Development of Eastern Poland 2007–2013, Priority Axis I Modern Economy, operations I.3 Innovation promotion. Calculations with Gaussian 09 were performed under a computational grant by Interdisciplinary Center for Mathematical and Computational Modeling (ICM), Warsaw, Poland, grant number G30-18 and under resources and licenses by CSC, Finland.

Open Access This article is distributed under the terms of the Creative Commons Attribution 4.0 International License (<http://creativecommons.org/licenses/by/4.0/>), which permits unrestricted use, distribution, and reproduction in any medium, provided you give appropriate credit to the original author(s) and the source, provide a link to the Creative Commons license, and indicate if changes were made.

References

- Dalpozzo R, Bartoli G, Bencivenni G. Recent advances in organocatalytic methods for the synthesis of disubstituted 2- and 3-indolinones. *Chem Soc Rev.* 2012;41:7247–90.
- Evans BE, Rittle KE, Bock MG, Dipardo RM, Freidinger RM, Whitter WL, Lundell GF, Veber DF, Anderson PS, Chang RSL, Lotti VJ, Cerino DJ, Chen TB, Kling PJ, Kunkel KA, Springer JP, Hirshfield J. Methods for drug discovery: development of potent, selective, orally effective cholecystokinin antagonists. *J Med Chem.* 1988;31:2235–46.
- Sharma V, Kumar P, Pathak D. Biological importance of the indole nucleus in recent years: a comprehensive review. *J Heterocycl Chem.* 2010;47:491–502.
- Kaushik NK, Kaushik N, Attri P, Kumar N, Kim CH, Verma AK, Choi EH. Biomedical importance of indoles. *Molecules.* 2013;18:6620–62.
- Chadha N, Silakari O. Indoles as therapeutics of interest in medicinal chemistry: bird’s eye view. *Eur J Med Chem.* 2017;134:159–84.
- Biswal S, Sahoo U, Sethy S, Kumar HKS, Banerjee M. Indole: the molecule of diverse biological activities. *Asian J Pharm Clin Res.* 2012;5:1–6.
- Bartoli G, Dalpozzo R, Nardi M. Applications of Bartoli indole synthesis. *Chem Soc Rev.* 2014;43:4728–50.
- Dalpozzo R. Strategies for the asymmetric functionalization of indoles: an update. *Chem Soc Rev.* 2015;44:742–78.
- Barden TC. Indoles: industrial, agricultural and over-the-counter uses. *Top Heterocycl Chem.* 2011;26:31–46.
- Kaczor AA, Kronbach C, Unverferth K, Pihlaja K, Wiinämäki K, Sinkkonen J, Kijkowska-Murak U, Wróbel T, Stachal T, Matusiuk D. Novel non-competitive antagonists of kainate GluK1/GluK2 receptors. *Lett Drug Des Discov.* 2012;9:891–8.
- Kaczor AA, Karczmarzyk Z, Fruziński A, Pihlaja K, Sinkkonen J, Wiinämäki K, Kronbach C, Unverferth K, Poso A, Matusiuk D. Structural studies, homology modeling and molecular docking of novel non-competitive antagonists of GluK1/GluK2 receptors. *Bioorg Med Chem.* 2014;22(2):787–95.
- Valgeirsson J, Nielsen EØ, Peters D, Varming T, Mathiesen C, Kristensen AS, Madsen U. 2-Arylureidobenzoic acids: selective noncompetitive antagonists for the homomeric kainate receptor subtype GluR5. *J Med Chem.* 2003;46:5834–43.
- Valgeirsson J, Nielsen EO, Peters D, Mathiesen C, Kristensen AS, Madsen U. Bioisosteric modifications of 2-arylureidobenzoic acids: selective noncompetitive antagonists for the homomeric kainate receptor subtype GluR5. *J Med Chem.* 2004;47:6948–57.
- Kaczor AA, Wróbel T, Kronbach C, Unverferth K, Stachal T, Matusiuk D. Synthesis and molecular docking of novel non-competitive antagonists of GluK2 receptor. *Med Chem Res.* 2015;24:810–7.
- Kaczor AA, Pihlaja K, Kronbach C, Unverferth K, Wrobel T, Stachal T, Matusiuk D. Synthesis and molecular docking of indole and carbazole derivatives with potential pharmacological activity. *Heterocycl Commun.* 2014;20:103–9.
- Kaczor AA, Matusiuk D. Molecular structure of ionotropic glutamate receptors. *Curr Med Chem.* 2010;17:2608–35.
- Stayte S, Vissel B. Advances in non-dopaminergic treatments for Parkinson’s disease. *Front Neurosci.* 2014;8:113.
- Crépel V, Mulle C. Physiopathology of kainate receptors in epilepsy. *Curr Opin Pharmacol.* 2015;20:83–8.
- Szénási G, Vegh M, Szabo G, Kertesz S, Kapus G, Albert M, Greff Z, Ling I, Barkoczy J, Simig G, Spedding M, Harsing LG Jr. 2,3-Benzodiazepine-type AMPA receptor antagonists and their neuroprotective effects. *Neurochem Int.* 2008;52:166–83.
- Kaczor AA, Kijkowska-Murak UA, Matusiuk D. Theoretical studies on the structure and symmetry of the transmembrane region of glutamatergic GluR5 receptor. *J Med Chem.* 2008;51(13):3765–76.
- Kaczor AA, Kijkowska-Murak UA, Kronbach C, Unverferth K, Matusiuk D. Modeling of glutamate GluR6 receptor and its interactions with novel noncompetitive antagonists. *J Chem Inf Model.* 2009;49:1094–104.

22. Jamróz MH. On the internal coordinates in the Potential Energy Distribution (PED) analysis: bending or torsion? *Environ Bioinform*. 2014;1:1–3.
23. Gaussian 09, Revision E.01, Frisch MJ, Trucks GW, Schlegel HB, Scuseria GE, Robb MA, Cheeseman JR, Scalman G, Barone V, Mennucci B, Petersson GA, Nakatsuji H, Caricato M, Li X, Hratchian HP, Izmaylov AF, Bloino J, Zheng G, Sonnenberg JL, Hada M, Ehara M, Toyota K, Fukuda R, Hasegawa J, Ishida M, Nakajima T, Honda Y, Kitao O, Nakai H, Vreven T, Montgomery JA Jr, Peralta JE, Ogliaro F, Bearpark M, Heyd JJ, Brothers E, Kudin KN, Staroverov VN, Kobayashi R, Normand J, Raghavachari K, Rendell A, Burant JC, Iyengar SS, Tomasi J, Cossi M, Rega N, Millam JM, Klene M, Knox JE, Cross JB, Bakken V, Adamo C, Jaramillo J, Gomperts R, Stratmann RE, Yazyev O, Austin AJ, Cammi R, Pomelli C, Ochterski JW, Martin RL, Morokuma K, Zakrzewski VG, Voth GA, Salvador P, Dannenberg JJ, Dapprich S, Daniels AD, Farkas Ö, Foresman JB, Ortiz JV, Cioslowski J, Fox DJ. Wallingford: Gaussian Inc.; 2009.
24. Barnes L, Schindler B, Allouche AR, Simon D, Chambert S, Oomens J, Compagnon I. Anharmonic simulations of the vibrational spectrum of sulfated compounds: application to the glycosaminoglycan fragment glucosamine 6-sulfate. *Phys Chem Chem Phys*. 2015;17:25705–13.
25. Jamróz MH. Vibrational energy distribution analysis VEDA 4, Warsaw; 2004.
26. Jamróz MH. Vibrational energy distribution analysis (VEDA): scopes and limitations. *Spectrochim Acta A*. 2013;114:220–30.
27. Pitucha M, Sobotka-Polska K, Keller R, Pachuta-Stec A, Mendyk E, Kaczor AA. Synthesis and structure of new 1-cyanoacetyl-4-arylsulfamicarbamide derivatives with potential anticancer activity. *J Mol Struct*. 2016;1104:24–32.
28. Bartyzel A, Kaczor AA. The formation of a neutral manganese(III) complex containing a tetradentate Schiff base and a ketone—synthesis and characterization. *J Coord Chem*. 2015;68:3701–17.
29. Kaczor AA, Bartyzel A, Pitucha M, Wróbel TM, Woźniak S, Matosiuk D. Synthesis, experimental and computational studies of *N*-(4-amino-6-oxo-1,6-dihydropyrimidin-5-yl)benzamide. *Lett Org Chem*. 2018. <https://doi.org/10.2174/1570178614666170811123851> (in press).
30. Bartyzel A, Kaczor AA. Synthesis, crystal structure, thermal, spectroscopic and theoretical studies of N₃O₂-donor Schiff base and its complex with Cu^{II} ions. *Polyhedron*. 2018;139:271–81.
31. Bartyzel A, Sztanke M, Sztanke K. Thermal studies of analgesic active 8-aryl-2,6,7,8-tetrahydroimidazo[2,1-*c*][1, 2, 4]triazine-3,4-diones. *J Therm Anal Calorim*. 2016;123:2053–60.
32. Bartyzel A, Sztanke M, Sztanke K. Thermal behaviour of antiproliferative active 3-(2-furanyl)-8-aryl-7,8-dihydroimidazo[2,1-*c*][1, 2, 4]triazin-4(6*H*)-ones. *J Therm Anal Calorim*. 2017;130:1541–51.
33. Bartyzel A. Effect of molar ratios of reagents and solvent on the complexation process of nickel(II) ions by the N₂O₃-donor Schiff base. *Polyhedron*. 2017;134:30–40.
34. Bartyzel A. Synthesis, thermal behaviour and some properties of Cu^{II} complexes with *N,O*-donor Schiff bases. *J Therm Anal Calorim*. 2018;131:1221–36.
35. Kanaoka Y, Ban Y, Oishi T, Yonemitsu O, Terashima M, Kimura T, Nakagawa M. Infrared spectra of some indole and pyrrole compounds. *Chem Pharm Bull*. 1960;8:294–301.
36. Sundaraganesan N, Umamaheswari H, Dominic Joshua B, Meganathan C, Ramalingam M. Molecular structure and vibrational spectra of indole and 5-aminoindole by density functional theory and ab initio Hartree–Fock calculations. *J Mol Struct Theochem*. 2008;850:84–93.
37. Saleem H, Subashchandrabose S, Erdogdu Y, Thanikachalam V, Jayabharathi J. FT-IR, FT-Raman spectral and conformational studies on (*E*)-2-(2-hydroxybenzylideneamino)-3-(1*H*-indol-3-yl) propionic acid. *Spectrochim Acta A*. 2013;101:91–9.
38. Bunte SW, Jensen GM, McNesby KL, Goodin DB, Chabalowski CF, Nieminen RM, Suhai S, Jalkanen KJ. Theoretical determination of the vibrational absorption and Raman spectra of 3-methylindole and 3-methylindole radicals. *Chem Phys*. 2001;265:13–25.
39. Arjunan V, Puviarasan N, Mohanc S. Fourier transform infrared and Raman spectral investigations of 5-aminoindole. *Spectrochim Acta A*. 2006;64:233–9.
40. Morzyk-Ociepa B. Vibrational spectroscopic studies of indole-carboxylic acids and their metal complexes Part VIII. 5-Methoxyindole-2-carboxylic acid and its Zn(II) complex. *Spectrochim Acta A*. 2009;72:236–43.
41. Mello GS, Cardoso AP, Oliveira EWRS, Siqueira AB. Tryptophan a proposal of the mechanism of thermal decomposition. *J Therm Anal Calorim*. 2015;122:1395–401.